Thermal Stresses and Physical Aging

Julie P. Harmon* and Charles L. Beatty, University of Florida

ENGINEERING PLASTICS, as a general class of materials, are prone to the development of internal stresses that arise during processing or during service when parts are exposed to environments that impose deformation and/or temperature extremes. These stresses, which manifest themselves in the properties of the plastic, may affect mechanical, optical, and electrical properties and may influence dimensional stability, permeability, and resistance to hostile environments. The effects may be beneficial or detrimental. It is possible, for example, to delay brittle fracture in plastic members by introducing residual compressive stresses on the surfaces of Izod impact specimens (Ref 1). On the other hand, the buildup of stresses during processing can result in voids or cracks that diminish mechanical properties.

Thermal stresses are largely a consequence of high coefficients of thermal expansion and low thermal diffusivities. These effects, which are exacerbated when there is a large difference between the glass transition temperature, T_g, and the ambient temperature, represent a problem in high-performance (high-temperature) thermoplastics such as polysulfone (PSU) or polyetherketone (PEK) because they develop significant thermal stresses upon cooling. It is this coefficient of thermal expansion (CTE) mismatch between polymers and fillers, especially anisotropic composites, that can lead to diminished mechanical properties. However, by a judicious choice of fillers, it is possible to lower the CTE of the composite to such an extent that it can be used in conjunction with metal parts, even at cryogenic temperatures. Although time-consuming techniques can be used to analyze thermal stresses, several useful qualitative tests will be described in this article.

Flow-induced orientation effects will also be discussed. Orientation commonly occurs in processing by such techniques as extrusion, injection molding, pultrusion, and calendering. The anisotropy of physical properties that accompanies orientation must be considered. Of paramount concern are the dimensional instabilities that arise from anisotropic CTEs.

Physical aging, which will also be examined, is the process by which plastics cooled below the T_g gradually approach thermodynamic equilibrium. The approach to equilibrium can lead to drastic or sometimes subtle changes in physical properties. Although aging is often characterized by monitoring changes in excess enthalpy and entropy, these measurements do not necessarily directly correlate with changes in physical properties. Aging temperature ranges have been determined for a number of plastics. It is accepted that the aging range extends from the T_g down to the highest secondary transition associated with small-scale molecular motion. Secondary transitions that are not well separated from the T_g or that involve cooperative motion are possible exceptions to this rule. At any rate, the densification and possible configurational changes that accompany aging alter mechanical properties, especially ductile-brittle behavior.

Cooling stresses, orientation, and the nonequilibrium thermodynamic state of glasses often simultaneously accompany processing. Orientation is removed by annealing above the T_g. The effect of thermal stresses can be somewhat isolated from aging effects by the layer removal technique. However, aging may also be affected by temperature gradients because material near the core of the sample is annealed for longer times. By being aware of these phenomena, an engineer should be able to select plastics and processing techniques more efficiently and to broaden product applications.

In an attempt to explain the stresses encountered in the plastics industry, the first section of this article will define the different types of internal stresses. Then, each type of thermal stress will be discussed in detail, with reference to the mechanism of generation and the effect on engineering properties. Methods of detecting and measuring internal stresses will be presented. Next, orientation effects will be described. Finally, numerous aspects of physical aging will be discussed.

Classification of Stress

Internal stress phenomena have been extensively studied in metals and inorganic glasses. The increased use of engineering plastics in structural materials has necessitated increasing the body of knowledge on this subject. Some excellent reviews in this area are available in the literature (Ref 2-4). There are three types of internal stresses in amorphous polymers (this classification scheme can be extended to include semicrystalline polymers and composites), as follows (Ref 4).

The first type, thermal or cooling stresses, results from rapid, inhomogeneous cooling through the T_g range in amorphous polymers or through the solidification range in semicrystalline polymers. When cooling proceeds from the outer layer inward, large thermal gradients are formed, and thermal stresses are frozen in. Thermal stresses also arise from the thermal mismatch between materials in a composite that have different thermal expansion properties.

The second type of internal stress consists of orientation and orientation stresses. Processing involves deformation at elevated temperatures. This deformation produces molecular orientation, which is accompanied by internal stresses. If cooling is rapid enough, these stresses are frozen in, along with orientation. This results in anisotropic physical properties and a propensity for dimensional instability.

The third type of internal stress includes quenching stresses and physical aging quenching stresses. These arise when an amorphous polymer is cooled to below the T_g at a rate that is too rapid for the molecules to attain a true glassy equilibrium state. Molecular motion below T_g is extremely slow, and the approach to the equilibrium state is a result of this slow motion. The approach to equilibrium gives rise to what is called physical aging. The net result is a slow contraction of material. This con-

*Currently a visiting scientist with affiliation at Eastman Kodak Company

traction relieves the internal stresses. The dimensional changes here are not as pronounced as those that result from the relaxation of thermal or orientation stresses. Nonetheless, mechanical properties are significantly affected by the aging process. Deformation by swelling can generate similar internal stresses.

Categorically, these three types of stresses are defined as separate entities. It is emphasized, however, that it is often difficult to isolate and quantify internal stresses in plastic parts. This is because the processing conditions may generate more than one type of internal stress; that is, orientation stresses are likely to be accompanied by cooling stresses.

Thermal Stresses

The buildup of cooling stresses in plastic parts is a result of the effects of low thermal diffusivity, high thermal expansion properties, and the variation of mechanical properties with temperature. An understanding of these properties and the way in which they compare with those of other classes of materials (inorganic glasses and metals) clarifies the fact that plastics are prone to the development of thermal stresses.

Thermal expansion can be defined in a number of ways (Ref 5):

- Specific thermal expansivity, in which $e = (\partial v/\partial T)_p$ in units of $cm^3/g \cdot °C$
- Volume CTE, in which $\alpha = 1/v\,(\partial v/\partial T)_p$ in units of 1/°C
- Linear CTE, in which $\beta = 1/L\,(\partial L/\partial T)_p$ in units of 1/°C

In the above cases, v is the specific volume, T is the temperature, and L is the length.

Thermal diffusivity is related to thermal conductivity (Ref 5):

- Thermal conductivity, λ, $= C_p \cdot \rho\mu \cdot L$ in units of $J/s \cdot m \cdot °C$
- Thermal diffusivity, D, $= \lambda/C_p \cdot \rho$ in units of cm^2/s

In these cases, C_p is the specific heat capacity at constant pressure, ρ is the density, and μ is the velocity of sound.

Table 1 lists room-temperature linear CTEs for various materials. It is apparent that plastics have large CTEs compared to those of metals or inorganic glass. However, the room-temperature thermal diffusivity, as given in Table 2, is much lower for plastics than for metals and is slightly lower than that of inorganic glass. It should be emphasized that the values listed in Tables 1 and 2 are room-temperature values. The CTEs and thermal diffusivities of plastics vary with temperature. In general, the variation in CTE with temperature above and below the T_g is not significant when compared with the large increase in the CTE that is encountered at T_g (Ref 5). The value of CTE of a glassy polymer is about one-half that of a liquid polymer (Ref 6). For crystalline polymers, the sharp increase in CTE occurs at the melting point. Values for glassy and crystalline components are approximately equal.

Table 1 Linear coefficients of thermal expansion

Material	10^{-6}/K
Polymethyl methacrylate(a)	50–90
Polyacrylonitrile(a)	66
Cellulose acetate(a)	100–150
Nylon 6(a)	80–83
Nylon 11(a)	100
Polycarbonate(a)	68
Polyethylene terephthalate(a)	65
Polyphenylene sulfide(a)	49
Polyethylene, branched(a)	100–220
Polypropylene(a)	81–100
Polystyrene(a)	50–83
Polyvinyl chloride(a)	50–100
Glass(b)	8.3–9.7
Gold(b)	14.3
Cast iron(b)	10.6
Carbon graphite(b)	7.9
Hardened stainless steel(b)	17.3

(a) Source: Ref. 6. (b) Source: Ref 7

The thermal conductivity of polymers goes through a broad maximum at T_g. For crystalline polymers, thermal conductivity increases with the percentage of crystalline and amorphous phases, ρ_c and ρ_a (Ref 5):

$$\frac{\lambda_c}{\lambda_a} \sim \left(\frac{\rho_c}{\rho_a}\right)^6 \qquad \text{(Eq 1)}$$

For the purpose of thermal stress determination, it is convenient to consider the thermal conductivity constant as the temperature varies.

Mechanical Properties Versus Temperature. Mechanical properties, specifically the Young's modulus, also vary with temperature. The glassy modulus of an amorphous polymer shows a large decrease as the polymer changes from the glassy to the rubbery state (Ref 4). The modulus of atactic polystyrene (PS) (M_n = 217 000) decreases 5000-fold in the transition region (Ref 9). There is less of a decrease at the glass transition in crystalline polymers. Crystalline isotactic PS showed a decrease in modulus by 400 times in the range from below T_g to near the melting temperature (Ref 9).

Table 2 Thermal diffusivity at room temperature

Material	Diffusivity, $cm^2/s \times 10^4$	Diffusivity, $in.^2/s \times 10^4$
Magnesium oxide(a)	1400	217
Iron(a)	2000	310
Glass(a)	20–60	3–9
Polypropylene(b)	9.5	1.5
Polystyrene(b)	11.1	1.7
Polymethyl methacrylate(b)	11.8	1.8
Polyvinyl chloride(b)	12.5	1.9
Polyethylene terephthalate	14.3	2.2

(a) Source: Ref 8. (b) Source: Ref 5

Solidification. Thermal stresses are due to inhomogeneous cooling during solidification. Solidification arises at such a temperature when the polymer matrix becomes stiff enough to support stress. This temperature occurs at the glass transition in amorphous thermoplastic and somewhat below the melting temperature in semicrystalline polymers (Ref 10).

The situation is somewhat different in cross-linked or thermoset processing. In this case, solidification takes place at the cure temperature because cross links enable the matrix to support stress (Ref 10). Unsaturated polyester and epoxy resins are included in this category. Stress support is a consequence of an increase in modulus that occurs as cooling proceeds through the T_g, below the melt temperature, T_m, or at the cure temperature. When thermoplastics or semicrystalline polymers are cooled from the outside in, the solidification temperature is reached rapidly at the surface of the mold. As cooling proceeds, the solidification boundary moves inward to the core. Compressive forces are generated at the surface of the mold by the solidifying internal layers. Internal layers are in a state of tension. The amount of contraction that takes place from the solidification temperature to the ambient temperature is determined by the CTE. In crystalline polymers, an additional volume decrease accompanies the crystallization process because crystalline fractions are denser than amorphous fractions.

The percentage of volume decrease that accompanies cooling from the solidification temperature to room temperature was measured for several polymers (Ref 10). The results are shown in Table 3. Potential volume changes are generally much higher for crystalline polymers than for amorphous thermoplastics. Inhomogeneous cooling inhibits the volume contraction in the inner layers of material when the solidification temperature is reached at the mold surface. The result is that the thermal stresses generated during cooling persist (become residual stresses).

In addition, crystallization against a cool mold surface produces an inhomogeneous semicrystalline morphology. The cool mold surface results in higher nucleation and growth rates, which produce a columnar spherulitic regime called the transcrystalline layer. The low thermal conductivity of the polymer melt allows steep temperature gradients to develop. The lower crystallization temperature at the surface, compared to the higher crystallization temperature of the interior, results in thinner lamellae, smaller-diameter spherulites, and a higher population of tie molecules. Therefore, the tensile strength and modulus of the trans-

Table 3 Percentage of volume decrease upon cooling

Material	Solidification temperature °C	°F	Volume contraction $\Delta V/V_0$, from solidification temperature, %
Polyethylene	120	274	22.0
Polyethylene terephthalate	200	418	13.6
Polycarbonate	160	346	3.2
Polysulfonate	185	391	3.2
Epoxy BP907	177	376	2.5

Source: Ref 10

crystalline layer are significantly higher than those of the interior.

Transcrystalline layer thicknesses of 1 to 20 μm (40 to 790 μin.) are not uncommon. In addition to this layered composite semicrystalline structure, the more rapid crystallization that occurs in the transcrystalline layer is subject to continued partial slow crystallization after removal from the mold. Therefore, the stress distribution in a molded semicrystalline polymer can be complex in terms of depth from the mold surface, the morphology obtained, and the time and temperature (that is, aging storage conditions) after the molding process.

Thermal Stress Distribution. Thermal expansion, thermal diffusivity, and the variation of mechanical properties with temperature are factors that engineers need to be familiar with in working thermal stresses. Struik (Ref 4) formulated a model for amorphous polymers encompassing these parameters. He modeled inhomogeneous cooling in flat sheets using thermoelastic theory. The main conclusions of this theory are:

- Stresses are proportional to A, which is defined as $A = \alpha E/(1-\nu)$, where α is the expansion coefficient, E is the Young's modulus of the glassy polymer, and ν is Poisson's ratio
- Stresses are determined by the temperature difference $T_0 - T_\infty$ and $T_g - T_\infty$, where T_0 is the initial temperature above T_g and T_∞ is the final temperature below T_g
- Stresses are further determined by $M = HL/$(thermal diffusivity), where M is the dimensionless Biot number, H is a convective heat transfer coefficient, and $2L$ is the sample thickness

In an effort to simplify the model, Struik neglected time-temperature effects on mechanical properties, volume relaxation effects, and nonlinear stress effects. Figure 1 shows a plot of residual stress distributions generated from this model. As the Biot number decreases, residual stresses decrease. This model makes apparent the factors that can be optimized in reducing residual thermal stresses:

- Select materials with lower glass moduli, or lower the CTEs
- Decrease convective heat transfer, that is, air cool instead of ice cool
- Increase thermal diffusivity. This results in more homogeneous cooling. It has been reported, for example, that thermal stresses are reduced by the incorporation of small amounts of conductive metal filler into the polymer matrix (Ref 8)

Thermal Mismatch. In composite structures, thermal stresses arise both from inhomogeneous cooling and as a result of thermal mismatch due to differences in CTEs between the filler and matrix polymer. Ideally, in terms of processing, one should attempt to minimize thermal stress buildup by minimizing the differences in CTEs. This is not always practical, because most fillers are inorganic materials with low CTEs.

Isotropic Effects. When spherical or particulate fillers are used, thermal contraction of the matrix exerts a compressive stress on the particle surface. This may actually be beneficial in that it can minimize decreases in the modulus due to poor filler-matrix adhesion (Ref 11). In extreme cases, however, cracking occurs, and the strength of the composite is diminished. The use of particulate fillers, especially spherical ones, offers the advantage of a lack of anisotropic shrinkage often found with fibrous fillers. In instances where polymers are joined with metal parts, it is desirable to decrease the CTE by the addition of filler to the polymer matrix. If the part is then exposed to extremes in temperature, the thermal mismatch between the filled polymer and metal surfaces is minimized, and thermal stresses are less likely to induce failure. In recent years there has been an increased use of filled polymers in cryogenic applications due to the ability to decrease CTEs by using fillers (Ref 12). For spherical fillers, the CTE of the composite is expressed as (Ref 11):

$$\alpha = \alpha_1 \phi_1 + \alpha_2 \phi_2 - (\alpha_1 - \alpha_2)\,\phi_1 \phi_2 \left[\frac{1/B_1 - 1/B_2}{\phi_1/B_1 + \phi_2/B_2 + 3/4G_1}\right] \quad \text{(Eq 2)}$$

where the subscripts 1 and 2 refer to polymer and composite, respectively; ϕ is the volume fraction; α is the CTE; B is the bulk modulus; and G is the shear modulus.

Powder-filled epoxy resin systems have been developed for use as spacers between superconductive cables in synchrotron accelerators (Ref 13). In this system, the part must withstand thermal cycling between room temperature and liquid helium temperature. The experimenters adjusted the thermal contraction of the epoxy matrix to match that of the cable by adding appropriate amounts of calcium carbonate, talc, or asbestos fillers. They used a model for predicting thermal contraction in polymer matrices filled with spheres (Ref 14). Thermal contraction is defined as:

$$\alpha = \frac{L_1 - L_2}{L_1} \quad \text{(Eq 3)}$$

where L_1 is the sample length at room temperature and L_2 is the sample length at liquid helium temperature.

Unfilled epoxy systems have a thermal contraction four times greater than that of the cable material. The experimenters succeeded in reducing the thermal contraction to match that of the metal without sacrificing the mechanical properties of the composite.

Anisotropic Effects. In the above example, filler-matrix contraction is isotropic. In fiber-reinforced composites, the CTEs of the fibers are anisotropic, and they are often layered anisotropically. As a result of this anisotropy, the effect of thermal stress may be more severe than that of powder-filled systems.

Two researchers studied the thermal stress buildup in unidirectional graphite- and aramid-filled composites (Ref 10). The longitudinal CTE for graphite is -0.36×10^{-6}/K; for aramid, -2×10^{-6}/K. The radial CTE for graphite is 18×10^{-6}/K; for aramid, 59×10^{-6}/K. The lower limit of thermal stress in the longitudinal direction was approximated as:

$$\sigma_\parallel = \frac{\Delta_\alpha E_m E_L V_f}{E_m V_m + E_L V_f}(T_0 - T) \quad \text{(Eq 4)}$$

where Δ_α is the difference in CTEs of the matrix and the fiber in the longitudinal direction, T is the temperature, T_0 is the

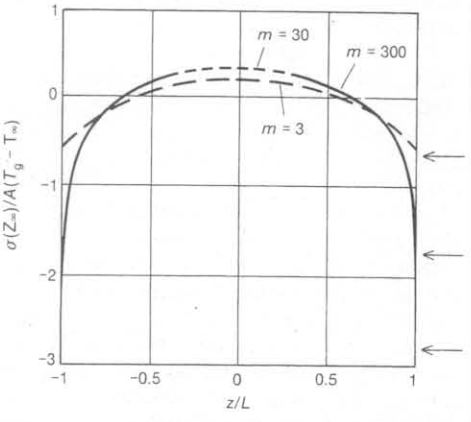

Fig. 1 Residual stress distributions for various values of m for the case that T_0 lies far above T_g. Source: Ref 4

Table 4 Thermal stresses

Principal stresses	Graphite/ polysulfone, $V_f = 0.33$	Graphite/ epoxy BP907, $V_f = 0.35$
$<\sigma_{\parallel} - \sigma_{\perp}>$, MPa (ksi)..	31.4 (4.5)	20.0 (2.9)
$<\sigma_{\parallel}>$, MPa (ksi).....	25.7 (3.7)	15.2 (2.2)
$<\sigma_{\perp}>$, MPa (ksi)	−5.7 (−0.8)	−4.8 (−0.7)

Source: Ref 10

solidification temperature, E_L and E_m are the longitudinal modulus of the fiber and the modulus of the matrix, and V_f and V_m are the volume fractions of fiber and matrix, respectively.

The researchers measured the average difference in principal stresses, $<\sigma_{\parallel} - \sigma_{\perp}>$, by photoelasticity, and from this they estimated the transverse stress, $\sigma_{\perp}$. The values are given in Table 4. Thermal stresses are obviously higher in the PSU composite than in the epoxy (EP) composite. This is because the volume contraction of PSU is higher than that of EP (Table 3). The laminates are molded at pressures from 0.34 to 3.4 MPa (0.05 to 0.5 ksi). In high-pressure molding (100 to 500 MPa, or 14.5 to 72.5 ksi), the volume contraction of the resin is decreased, and thermal stresses are likely to be less severe.

The situation becomes more complex when one considers anisotropic fiber arrays. Laminates are often formed from layers of unidirectional plies, the direction of the plies being rotated to increase strength. Two types of residual thermal stresses develop: microstresses around each fiber and macrostresses between the plies.

One researcher used strain gages to measure directional expansion coefficients in unidirectional- and angle-ply laminates (Ref 15). Residual strains were measured from differences in the coefficients between angle-ply and single-ply laminates for particular directions in relation to the fibers. Residual stresses were calculated directly from these residual strains. In graphite-epoxy and aramid-epoxy laminates, residual stresses at room temperature exceeded the transverse tensile strength of the unidirectional composite. In addition, these stresses did not relax with time. Residual stresses and the tendency toward cracking were strongly dependent on ply lay-up. Transverse stresses increased from zero to a maximum as the angle between the two plies varied from 0 to 90°. Although ply rotation can be optimized to yield a zero net expansion coefficient, this may result in a considerable buildup of thermal stresses.

Thermal Stress Measurement. Thermal stresses can be determined quantitatively by complex, time-consuming methods. However, it is often more practical for the engineer to use qualitative methods to estimate the severity of the problem.

Methods developed for determining thermal stresses in metals have been adapted for use with polymers. One researcher proposed a method of estimating the average internal stress in a cross section of metal by stress relaxation (Ref 16). In stress relaxation tests, strain is kept constant, and stress decay is monitored as a function of time. Other researchers suggested a method of analyzing stress relaxation data to obtain the average internal stress, σ_i (Ref 8, 17, 18). The maximum slope of a stress log time plot, F, is determined by:

$$F = -\left(\frac{d\sigma}{d \log t}\right)_{max} \quad \text{(Eq 5)}$$

A plot of F versus initial stress, σ_0, yields a straight line, intersecting the σ_0 axis at a value equivalent to the internal stress. This method is time consuming and yields only an average stress rather than a stress profile (Ref 2, 19).

The layer removal technique is useful in measuring residual stress distributions. It is applicable in a practical sense only to flat bars, plates, and pipes (Ref 2). Thin layers are removed from one face of the sample with high-speed milling machines. The face becomes unbalanced, and the sample takes on a curvature, ρ. A plot of curvature versus depth of removed material can be converted into a stress versus depth profile. Formulas for stress distributions using the layer removal technique are reviewed in Ref 2, and applications of this technique are abundant in the literature (Ref 1, 19, 20, 21).

For the case of a rectangular bar with no directional effects in the plane of the specimen (Ref 22):

$$\sigma_x(Z) = \sigma_y(Z) = \frac{-E}{6(1-\nu)}\left[(Z_0 + Z_1)^2 \frac{d\rho x(Z_1)}{dZ_1} + 4(Z_0 + Z_1)\rho x(Z_1) - 2\int_{Z_1}^{Z_0} \rho x(Z)\, dZ\right] \quad \text{(Eq 6)}$$

where E is the elastic modulus, ρx is the curvature parallel to the x direction, $Z = \pm Z_0$ are the original upper and lower surfaces, and Z_1 is the upper surface after layer removal.

As a word of caution, layer removal techniques assume that no gradient in modulus exists throughout the specimen thickness. However, density and modulus increase in the direction from the sample edge to the core (Ref 22, 23). This effect is more complex in oriented specimens, as discussed in the following section.

Unbalanced forces may result in curvature in unbalanced cross-ply laminates or in coatings cured on metal substrates (Ref 24, 25). Thermal stresses and strains have been related to the curvature in such systems. In processing simulated laminates, plies are separated by a release ply that is removed after cooling. Internal stresses are analyzed in terms of the deformation that occurs upon separation (Ref 26).

Thermal Stress Evaluation. The engineer is often faced with the need to use less rigorous qualitative techniques. Microscopy may be valuable in revealing the presence of voids or cracks induced by thermal stresses and possible skin-core or crystalline morphology changes in molded parts (Ref 2, 19).

A number of qualitative techniques are given in Ref 8. Surface hardness, for example, decreases because of internal tensile stresses and increases for compressive stresses. The researchers (Ref 8) suggest a method for assessing the effect of internal stress on cracking tendencies. Here, a hole is drilled in the sample, and the sample is exposed to certain liquids. When such a sample of PS was placed in contact with *n*-hexane, samples with lower internal stresses showed less cracking. Also, they correlated shrinkage to thermal stresses: $\epsilon_s = (\alpha_m - \alpha_s)/\alpha_m$, where ϵ_s is the mold shrinkage, α_m is the length dimension of the mold cavity, and α_s is the sample length. They noted a decrease in mold shrinkage in metal-filled samples. Modulus, tensile strength, and elongation-to-rupture usually show a weak dependence on internal stress level. (Of course, only average values of these parameters are measured when a tensile specimen is pulled if the gradient in properties in the thickness direction is not taken into account.) The above methods for evaluating thermal stresses are, again, complicated by concurrent aging and orientation effects in processed parts.

Orientation Effects

As mentioned earlier, processing at elevated temperatures often results in residual orientation upon cooling to below T_g. Struik has shown (Ref 4), by using a model for rubber elasticity and the theory of the kinetic origin of rubber elasticity, that molecular orientation is accompanied by residual entropy stresses. Orientation and entropy stresses affect anisotropy effects. For example, the linear CTE depends on the direction of orientation, while the volume CTE for oriented and unoriented material is the same:

$$\alpha = \beta_{\parallel} + 2\beta_{\perp} \quad \text{(Eq 7)}$$

where $\beta_{\parallel}$ and $\beta_{\perp}$ are linear CTEs parallel and perpendicular to molecular alignment (Ref 5). Orientation-induced anisotropy is also evident in small-strain mechanical properties, creep, and yield behavior. The characterization of orientation and the effects of orientation on physical properties are discussed in Ref 27 to 31.

Of interest here are the more complicated, combined effects of thermal stresses and orientation that result from processing conditions. One of the most straightforward ways of separating these effects is to measure residual stresses in a processed part that has orientation and residual thermal stresses and to compare these results with identical specimens that are heated above the T_g to remove orientation and then quenched. The latter gives information on the thermal stress profile only.

The residual thermal stress profile for flat sheets (Fig. 1) is parabolic, with the compressive stresses on the surface and the core in tension. A team of researchers characterized residual stresses in injection-molded parts where flow-induced stresses and orientation accompany thermal stresses (Ref 23, 32, 33). Flow-induced tensile stresses maximize at the mold surface. When combined with thermal stresses, compression stresses on the surface are reduced. Extreme conditions inducing orientation result in tensile stresses at the surface.

The researchers investigated the effect of melt temperature, injection pressure, injection time, and mold temperature on residual stresses as determined by the layer removal technique. Curvature measurements were taken in the direction corresponding to stresses parallel to the flow direction. Polyphenylene oxide (PPO), PSU, and an amorphous polyamide (PA) were studied.

The conclusions of this work depict the effect of processing-induced orientation and residual stresses on mechanical properties, especially tensile strength, ultimate elongation, and elastic modulus. When melt and mold temperatures were optimized for each polymer, PPO and PSU showed an increase in modulus parallel to the injection direction as the injection rate increased (Ref 32, 33).

The ultimate properties of PSU were measured. Increasing the injection rate increased the ultimate strength and decreased the elongation-to-break. The decrease in the latter is associated with an increase in orientation parallel to the deformation axis. Increasing the injection pressure had similar effects on the ultimate elongation of PSU.

Polyamide samples were studied in more detail; that is, tensile properties were measured after successive layer removals on both sides. A distinct gradient in mechanical properties was noted. The elastic modulus increased with increasing injection pressure, and as the remaining sample thickness increased at low temperatures, ultimate properties increased toward the center of the sample; the opposite occurred at higher pressures.

It is interesting to note that in thermally treated and quenched PPO samples, gradients in the tensile properties increased upon approach to the center of the sample (Ref 22, 23). Density increases paralleled this effect. This may be due to the need to consider aging effects. Aging effects are more pronounced in the inner layers of the sample, which cool at slower rates. Apparently, orientation and flow-induced stresses reverse this effect.

The failure properties of anisotropic molded parts are also anisotropic. It has been shown that the fracture energy of nylon 11 varies with respect to the flow direction in injection-molded samples (Ref 34). Notched Charpy impact tests at room temperature at a constant set hammer speed indicated that fracture occurs in stable and unstable propagation stages, each associated with a strain energy release rate. The strain energy release rates for both stable and unstable crack propagation are higher (by a factor as much as 1.2) perpendicular to the flow direction. This is attributed to anisotropic craze resistance. This resistance is higher in the flow, or orientation, direction.

Processing-induced anisotropy also increases susceptibility to hostile environments. For example, extruded in-line drawn PS samples sorb hydrocarbons at accelerated rates transverse to the orientation direction. Such oriented samples also show increased dissolution rates (Ref 35).

This indicates that processing induces complex orientation and residual stress effects. In analyzing these effects, sample orientation with respect to the flow directions and gradients in successive sample layers must be taken into account. Residual stress calculations by the layer removal technique must consider variations in the modulus, which occur in both annealed-quenched specimens and as-is injection-molded specimens.

Physical Aging

Physical aging at temperatures below the T_g has been extensively studied in linear amorphous polymers (Ref 3, 4, 36-39). This work has been extended to include cross-linked (Ref 37, 39) and filled (Ref 37, 40) polymers. It is speculated that aging occurs above the T_g in crystalline polymers because of the pinning action of crystalline components, which retard mobility (Ref 19). Aging is also known to occur in inorganic glasses and polycrystalline metals (Ref 3, 37). Of primary concern to the engineer is the fact that the onset of aging occurs when the polymer is cooled to the T_g and may continue for long periods of time, during which there is a simultaneous change in mechanical properties. Especially critical is that aging may have a profound effect on failure properties.

Thermodynamic Equilibrium. When cooled through the T_g, polymers behave like undercooled liquids; that is, they are not at thermodynamic equilibrium. As a result, the structure of the glassy polymer is continually changing in the course of the approach to the thermodynamic equilibrium state. This is best understood qualitatively from the concept of free volume (Ref 19). The nonequilibrium state is associated with free volume, which is accessible for molecular rearrangements. The approach to equilibrium is accompanied by a decrease of free volume, which then limits mobility and, therefore, rearrangement. The process of aging, at least in part, is associated with gradual densification of the material. This structural packing in turn causes the material to become more brittle (Ref 41).

The nonequilibrium state results in excess enthalpy, entropy, and volume. Physical aging has been characterized by decreases in excess volume and enthalpy (Ref 36, 38, 42-45). Although both quantities qualitatively parallel changes associated with aging, no quantitative relation to the free energy of the system has been found (Ref 46).

In volume relaxations, the typical increase in density is of the order of 0.5% (Ref 47). The most convenient method of recording changes in volume of this magnitude is volume dilatometry. Volume changes determined by this method are reported to have an accuracy of 1 to 5×10^{-5} cm^3/g (0.6 to 3×10^{-3} ft^3/lb). The use of the dilatometer is discussed in Ref 37 and 48.

One researcher measured the isobaric volume recovery in PS samples quenched from a temperature above T_g to temperatures below T_g (Ref 23). He developed a phenomenological theory to account for behavior such as this based on a distribution of retardation times (Ref 42). The model encompassed material constants and retardation spectra. It accurately predicted the response of glassy polymers to thermal treatments.

Another researcher proposed a mechanism for volume relaxation based on defect annihilation (Ref 49). If positive and negative density defects or excess volumes combine during annealing, volume recovery follows second-order kinetics. By assuming that $V - V_\infty$ is proportional to the concentration of defects at time, t, he observed second-order kinetics at long aging times.

In another experiment, a researcher monitored enthalpy relaxations by differential scanning calorimetry (DSC) (Ref 38, 43, 44). Briefly, enthalpy relaxation is accompanied by an absorption of energy or an endotherm in the region of the glass transition. Aging also shifts the position of the glass transition to higher temperatures. The energy absorbed increases with annealing time and approaches a maximum characteristic of each annealing temperature. Figure 2 shows typical endotherms resulting from annealing epoxy (EP) at times ranging from 0 to 52 000 min at 23 °C (73 °F). Measurements were taken with a differential scanning calorimeter at a heating rate of 10 °C/min (18 °F/min).

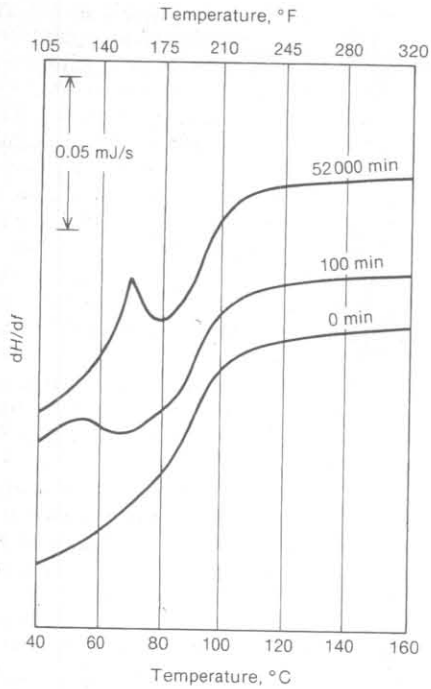

Fig. 2 Annealing time effects on DSC traces of epoxy 828-0-0. Annealed at 23 °C (73 °F). Source: Ref 39

The area under the curve represents the difference in enthalpy between initial and final temperatures. The area difference between that of the quenched sample (0 time) and that for a particular aging time gives a quantitative value for the enthalpy relaxation (Ref 39).

Aging and Physical Properties. The engineer is concerned with determining the effect of aging on mechanical properties and the susceptibility to solvent or corrosive environments. Changes in thermodynamic properties induced by aging can only be related qualitatively to changes in mechanical properties. The measurement of volume relaxation, for example, will not provide information that can quantitatively predict the effect of aging on yield stress or elongation-to-break. Aging is commonly interpreted in terms of a shift in relaxation times. Because rearrangements on the molecular scale involve more than one mode of motion, a spectrum or distribution of relaxation times is used to model aging phenomenon. A primary effect of aging is a shift of the intrinsic relaxation time distribution to longer times. Enthalpy and volume recovery are best characterized by a broad distribution of relaxation times. Such broad distributions, however, predict that the effect of aging on mechanical properties is sluggish compared to experimental results (Ref 50).

General Effects of Aging on Mechanical Properties. The effects of aging on mechanical properties, especially creep behavior, have been extensively studied by Struik (Ref 3, 37). Figure 3 shows a series of tensile creep curves for polyvinyl chloride (PVC) quenched from 90 to 40 °C (195 to 105 °F). The creep curve shifts by 4.5 decades in aging from 0 to 1000 days (Ref 3). For a fixed time, the magnitude of the compliance changes by almost 50%. Such creep curves can be superimposed by a horizontal shift, indicating that aging is related to relaxation time changes. This horizontal shift, log a, varies linearly with log t_e, where t_e is the aging time. This is expressed as an aging shift rate:

$$\mu = \frac{\mathrm{d} \log a}{\mathrm{d} \log t_e} \qquad \text{(Eq 8)}$$

Above T_g, where no aging occurs, μ is 0. At the T_g and throughout the aging range, μ is unity. This is the case for most polymers with relatively flexible chains. Polymers such as cellulose-acetate-butyrate (CAB) have rigid backbone structures. CAB has a maximum μ value of 0.75 (Ref 51). This is attributed to the inability of the rigid structure to age as well as more flexible structures.

Another phenomenon associated with aging is thermoreversibility. In an experiment similar to that shown in Fig. 2, a sample was reheated after 1000-day aging. It was then quenched and aged for 1 day. The creep curve for this sample superimposed the creep curve for the original 1-day aging curve (Ref 3).

This extensive work in the area of aging has led to a characterization of basic aging aspects, some of which are (Ref 3):

- Aging affects the long-term behavior of plastics. Aging time is the main parameter that affects small-strain properties
- In the aging range, all polymers age the same. The small-strain behavior of PS, for example, is similar to that of polycarbonate (PC) and other glassy structures
- Aging is a general phenomenon; it has been observed in all glassy structures, such as bitumen, shellac, amorphous sugar, and molded dry cheese powder
- Aging persists for long periods of time. If t_∞ is the time required to reach equilibrium glass structure at a temperature T below T_g, t_∞ increases by about a factor of ten per 3 °C (5 °F) in $T_g - T$
- Aging occurs at temperatures from T_g down to the temperature of the highest secondary transition associated with localized rather than segmental motion. Below this temperature, aging appears to cease

Ductile-Brittle Behavior. In reference to this last point, the magnitude of the temperature range from the local mode transition to the glass transition is also an indication of the temperature range over which a polymer exhibits ductile versus brittle behavior. Polymers, such as PC, with broad aging temperature ranges will exhibit ductility over a broad range in temperatures. The converse is true of PS and polymethyl methacrylate (PMMA).

The work on aging done by Struik has shed new light on ductile versus brittle behavior. It should be mentioned that such behavior is characterized by a ductile-to-brittle transition temperature. This temperature is not a material property; instead, it depends on the strain rate and the imposed stress configuration. As the strain rate increases, the ductile-to-brittle transition shifts to higher temperatures. At this transition temperature, there is competition between the ductile mode of failure (shear banding) and the brittle mode of failure (crazing) (Ref 52). At a particular strain rate, then, polymers exhibit ductile behavior over a range of temperatures, $T - T_g$,

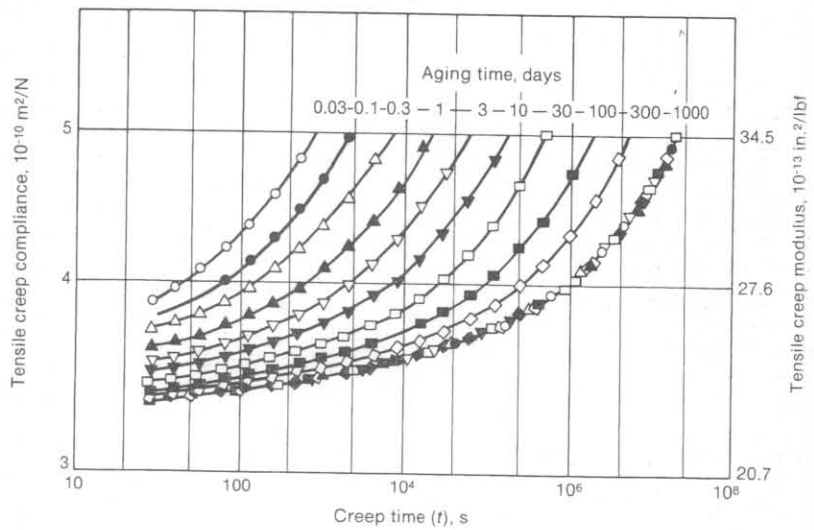

Fig. 3 PVC quenched from 90 to 40 °C (195 to 105 °F). Accurate to ±2%. Source: Ref 37

the breadth of which increases as the aging temperature range increases.

In the past, it was thought that secondary transitions were responsible for enhancing ductility in polymers. In some cases, there were direct correlations between ductile behavior and secondary transitions, but this observation does not extend to all polymers. This topic is discussed in Ref 53. More recent studies indicate that aging has a profound influence on ductile versus brittle behavior. Both aging and ductility are believed to require some segmental mobility (Ref 3). Below the secondary transition, there is no segmental mobility, and both ductile behavior and aging cease.

Aging and Transition Behavior. Dielectric and dynamic mechanical spectroscopies reveal the effects of aging in relation to primary and secondary transitions. Quenched polymers exhibit higher damping than slow-cooled or annealed polymers. The T_g is also lower in quenched specimens. There is evidence that quenching decreases the modulus (Ref 54). Of interest is the fact that quenching broadens the low-temperature end of the damping peak for the glass transition. Because aging is associated with main-chain or segmented motion, it is important to know whether or not the broadening of the glass transition damping peak extends into regions encompassing or affecting the secondary transition region (Ref 3).

Two researchers monitored the effect of cooling rate on primary and secondary transitions in amorphous methacrylate polymers by dielectric relaxation (Ref 55). The polymers investigated were PMMA, polyethyl methacrylate (PEMA), polybutyl methacrylate (PBMA), and polyisobutyl methacrylate (P-iso-BMA). They found, in general, that annealing lowered damping in regions below T_g and above the secondary transition. Previously, they reported that in some cases quenching resulted in the appearance of a new damping peak between these two transitions (Ref 56).

In PEMA, PBMA, and P-iso-BMA, the secondary transition is well separated from the glass transition. They found that the region below T_g affected by quenching was constant, irrespective of frequency (frequencies were varied from 60 Hz to 50 kHz), even though the β peak moved to higher temperatures according to the activation energy. This indicates the volume contraction effects, mainly segmental motion. Effects are not discernible in polymers where the damping peaks of the T_g and secondary transition overlap. This is the case with PMMA. Secondary transitions have a much lower activation energy than the glass transition. Consequently, the secondary peak shifts with frequency at a more rapid rate, merging with T_g at higher frequencies. At 60 Hz, annealing effects were apparent in the relaxation spectrum of PMMA. At higher frequencies, when the damping peaks merged, no annealing effects were apparent. As mentioned earlier, PMMA has a much smaller aging temperature range than other amorphous polymers, such as PC.

Aging and High-Strain Behavior. Aging effects are apparent in small-strain creep experiments and in mechanical and dielectric measurements. In considering the failure of plastic parts, it is important to extend aging studies to include effects due to higher deformations.

Creep rates have been examined by Struik at stresses that induce nonlinear deformation (Ref 37). At higher deformations, the aging effect is erased. Nonlinear creep curves were shifted to the right as aging time increased. The shifting appeared to be horizontal in the samples examined. The shift was still characterized by the double logarithmic shift rate, μ, which decreases with increasing stress. Nevertheless, the shift was the same for the polymers investigated. Both shear and tensile deformations were examined. The shift, again, was independent of the type of deformation.

In a study of nonlinear deformations and physical aging in PMMA, two researchers measured the torque and normal force in stress relaxation tests for different aging times (Ref 57). They found that from 40 to 60 °C (105 to 140 °F) the aging curves for linear, small-strain deformations could not be superimposed by horizontal and vertical shifts. At higher temperatures or at deformations in the nonlinear range, the curves were superimposed by a horizontal shift. Shifts decreased as the strain increased. In addition, shift rates were significantly lower for torque than for normal force measurements. It has been suggested that torque measurements are less sensitive than normal force measurements to aging-induced structural rearrangements. Large deformations may also affect the structure in such a way that torque and normal force measurements respond differently. The inability to superimpose data by a horizontal shift factor is due to possible contributions from the secondary relaxation process. Again, PMMA has a short aging range. It is worthwhile to investigate a broader range of polymers by this method of testing.

In recent years, mechanical testing has evolved to such an extent that large-strain behavior can be probed by very sensitive techniques. This is done by the superposition of small stresses or strains onto large stresses. These techniques depict the erasing of aging that follows large deformations. A group of researchers examined the behavior of PMMA by such a technique (Ref 58). They used torsional microcreep to monitor the effect of aging time on creep behavior. On aged specimens, they applied increasing longitudinal stresses and simultaneously measured microcreep. Microcreep alone clearly depicted the aging. In the early stages of microcreep (200 to 1200 s) at 90 °C (195 °F), microcreep was logarithmic:

$$\gamma_l = A\tau \ln \alpha t \qquad \text{(Eq 9)}$$

where γ_l is the strain, A is the constant that characterizes strain rate, τ is the stress, $\alpha = 10$ and is a constant to account for time of stress application, and t is time.

After this stage, microcreep reached a stable strain rate characterized by:

$$\dot{\gamma}_s = B\tau \qquad \text{(Eq 10)}$$

During logarithmic creep, the effect of aging time, t_e, on the constant, A, followed the form:

$$10^{11} A = 1.02 \log t_e + 4.92 \qquad \text{(Eq 11)}$$

The parameter B appeared to decrease with t_e in a logarithmic fashion. Both parameters characterize strain rate. The logarithmic decrease with t_e is thought to be analogous to the horizontal shift discussed by Struik. When a series of increasing longitudinal stresses was applied during microcreep on one aged sample, the parameters A and B decreased with stress increase in an opposite fashion to those in the aging study. This effect was noted only at longitudinal strains greater than 1%. This indicates that the structure that evolves during high-strain deformations is similar to that in quenched, unaged samples.

High-strain deformations are also found to influence aging in yield stress measurements. It has long been known that tensile, flexural, torsional, and compressive yield stresses increase with aging (Ref 37, 38, 59, 60). Plots of yield stress versus logarithm of strain rate for various aging times show behavior similar to that of small-strain creep behavior (Fig. 3). The magnitude of the shift is, again, much smaller than that in small-strain experiments (Ref 37). Also of importance is whether or not aging shifts the mode of failure from yield to brittle fracture. An excellent example of this is shown in Fig. 4. Aged and unaged amorphous polyethylene terephthalate (PET) was pulled in tension at a strain rate of 10%/min. Aging for only 90 min at 50 °C (120 °F) resulted in brittle behavior. Aging at room temperature for only 4 days produced the same effect (Ref 44).

The effect of aging on a yield or embrittlement is not always only an effect of a decrease in the volume due to aging. Intramolecular and intermolecular conformations influence the effect of aging on deformation. A team of researchers studied the effect of PC structure on high-deformation behavior and aging (Ref 47). The polymers used were bisphenol A polycarbonate, polyester carbonate with varying ratios of terephthalate and isophthalate esters, bisphenol A/phenophthalein random copolycarbonate, and PSU.

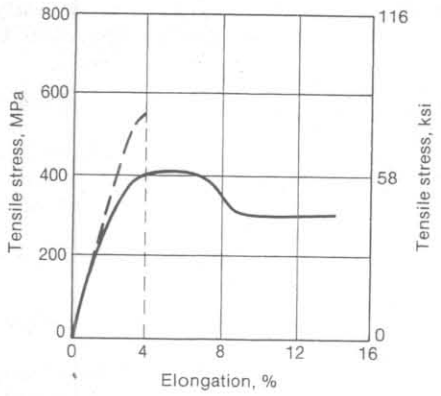

Fig. 4 Tensile stress-strain curves for amorphous PET film unannealed (solid line) and annealed at 51 °C (125 °F) for 90 min (dashed line). Source: Ref 44

The effect of aging on density was monitored by dynamic mechanical spectroscopy. This technique revealed a secondary transition in PCs at around 70 °C (160 °F). This transition is believed to be due to a cooperative motion of three to four monomer units and is therefore not highly localized.

Stress-strain curves for the samples showed a postyield stress drop. This stress drop decreased with increasing damping peaks associated with the secondary transition. Aging increased the postyield stress drop and decreased the height of the damping peak. Increasing T units increased peak height and decreased the stress drop. The magnitude of this stress drop is an indication of the amount of conformational change and packing that is unfavorable for ductile deformation. Damping peak heights also correlated with time-to-embrittlement due to aging for a particular strain rate. The higher the peak height, the greater the resistance to embrittlement. Densities showed a decrease with aging, but these data did not correlate with embrittlement data. This is an indication that both free volume and conformational changes take place during aging-induced deformation effects.

The effect of aging on the degree of ductility is further depicted in shear band studies. Shear banding is a form of inhomogeneous deformation observed in compression studies. It has been well characterized in polymers such as PMMA, PS, PET, and PC (Ref 43, 61-65). Shear yield induces the formation of two types of slip bands: coarse and fine. Temperature, strain rate, and aging influence the type of band formed. Higher temperatures, slower strain rates, and decreased aging favor the formation of the more diffuse fine bands. Fine bands induce ductile fracture after large deformations, while coarse bands induce brittle fracture after propagating through the specimens. Annealing increases the tendency to form coarse bands (Ref 61). This is yet another demonstration of the effect of aging on embrittlement.

As expected, aging influences other high-strain properties as well. Aging induces a decrease in strain-to-break for rubber-modified and pure epoxy systems (Ref 39). Similarly, in graphite-epoxy complexes, decreases in tensile strength, toughness, and strain-to-break accompanied increases in aging times (Ref 40).

Other effects of aging on materials extend beyond the realm of density increases and mechanical properties. Of particular importance to the engineer is the influence of aging on the susceptibility to solvent or swelling environments. For example, it has been shown that annealing decreases the diffusion coefficient of methane and propane in glassy polymers (Ref 66). Here, the vapor concentration was low enough so that swelling did not occur. Another researcher studied the effect of annealing on the sorption of *n*-hexane in glassy polymers (Ref 67). Annealing decreased sorption rates by factors as high as 100. Equilibrium solubilities were unaffected. It is important, then, to consider the thermal history of polymer parts that are exposed to such environments.

Appendix: Use of High-Modulus Graphite Fibers in Amorphous Polymers

High-modulus graphite fibers impart strength to composites. However, thermal stresses build up during processing in the temperature range from solidification to ambient temperature. If the structures survive in this temperature range, the question arises as to how far these structures can be cooled before thermal stresses cause failure.

In this study, six amorphous polymers are examined for suitability in graphite composites. The longitudinal stress due to the presence of the fiber is calculated for different temperature ranges, ΔT, from the solidification temperature T_0 to T_f, where T_f is the room temperature, liquid nitrogen temperature, or liquid helium temperature. The longitudinal tensile stress is significantly higher than the transverse stress and is therefore likely to be the stress controlling the failure. The compressive strength of amorphous polymers is also greater than the tensile stress. The stress, $\sigma_{\parallel}$, is calculated as follows (Ref 10):

$$\sigma_{\parallel} = \frac{\Delta_\alpha E_m E_L V_f}{E_m V_m + E_L V_f}(T_0 - T) \qquad \text{(Eq 12)}$$

where the symbols are as defined for Eq 4, and $E_m = 220$ GPa (32×10^6 psi). If $E_L \gg E_m$ (as is the case with graphite fibers as compared to amorphous polymers), then Eq 12 can be approximated as (Ref 10):

$$\sigma_{\parallel} = \int_{T_f}^{T_0} \Delta\sigma \, E_m \, dT \qquad \text{(Eq 13)}$$

Because $\sigma_{\parallel}$ is actually a lower limit of residual stress (Ref 10), a safety factor should be used when considering failure. For the purpose of comparison, the safety factor is eliminated.

The relevant properties of the polymers are shown in Table 5. Table 6 shows calculated values of $\sigma_{\parallel}$ versus the tensile strength of the polymer. In these calculations, a modulus invariant with temperature is assumed. The calculations are valid for V_f at 10% and greater. Above 10%, $\sigma_{\parallel}$ is constant (Ref 10).

The $\sigma_{\parallel}$ values for cooldown from solidification temperatures to room temperature indicate that the polymer matrix is likely to remain intact. Upon cooling to liquid nitrogen or liquid helium temperature, it is doubtful that any structures would hold up. The EP compound is the closest to being able to withstand these temperatures. Advances in EP chemistry have resulted in stronger epoxy compounds. This is one approach to the problem of expanding the useful temperature range for graphite-epoxies. In addition, it is possible to use a combination of two fillers: a spherical filler and a fiber. The spherical filler reduces the

Table 5 Properties of polymers

Material	Linear coefficient of thermal expansion, 10^{-6}/K	Tensile modulus GPa	Tensile modulus 10^5 psi	Tensile strength MPa	Tensile strength ksi	Temperature solidification °C	Temperature solidification °F
Polymethyl methacrylate	70	2.76	4.00	65.6	9.5	97	207
Polyacrylonitrile	66	3.76	5.45	62.0	9.0	95	203
Polycarbonate	68	2.38	3.45	65.6	9.5	150	302
Polystyrene	63	2.77	4.02	42.8	6.2	102	216
Polyvinyl chloride	75	3.27	4.75	46.9	6.8	80	176
Cast epoxy	55	2.41	3.50	58.7	8.5	170	338

Source: Ref 6

Table 6 Calculated values of $\sigma_{\parallel}$ versus tensile strength of various polymers

Material	Tensile strength MPa	Tensile strength ksi	$\sigma_{\parallel}$ Cool to room temperature MPa	$\sigma_{\parallel}$ Cool to room temperature ksi	$\sigma_{\parallel}$ Cool to liquid nitrogen MPa	$\sigma_{\parallel}$ Cool to liquid nitrogen ksi	$\sigma_{\parallel}$ Cool to liquid helium MPa	$\sigma_{\parallel}$ Cool to liquid helium ksi
Polymethyl methacrylate	66	9.5	15	2.1	57	8.3	71	10.3
Polyacrylonitrile	62	9.0	18	2.6	73	10.6	90	13.1
Polycarbonate	66	9.5	21	3.0	57	8.2	68	9.9
Polystyrene	43	6.2	14	2.0	52	7.6	66	9.5
Polyvinyl chloride	47	6.8	14	2.0	44	6.4	86	12.5
Epoxy	59	8.5	19	2.8	35	5.1	59	8.5

expansion coefficient with less residual stress effects. This reduction in σ_c is calculated from the linear rule of mixtures (Ref 11):

$$\sigma_c = \phi_1 \sigma_1 + \phi_2 \sigma_2 \qquad \text{(Eq 14)}$$

where ϕ is the volume fraction and the subscripts 1 and 2 refer to matrix and fillers. Equation 14 is a close approximation. Figure 5 shows a plot of σ_c versus volume fraction of filler for three representative polymers. For EP, a 30% level of filler significantly reduces σ_c.

Residual stress modeling in three-component systems is complicated. Nonetheless, calculations such as those in Table 6 give the engineer an approximate direction in which to proceed.

REFERENCES

1. P. So and L.J. Broutman, Residual Stresses in Polymers and Their Effect on Mechanical Behavior, *Polym. Eng. Sci.*, Vol 6 (No. 12), Dec 1976, p 785
2. J.R. White, Origins and Measurement of Internal Stress in Plastics, in *Measurement Techniques for Polymer Solids*, R.P. Brown and B.E. Read, Ed., Elsevier, 1984, p 165
3. L.C.E. Struik, Physical Aging in Plastics and Other Glassy Materials, *Polym. Eng. Sci.*, Vol 17 (No. 3), March 1977, p 165
4. L.C.E. Struik, Orientation Effects and Cooling Stresses in Amorphous Polymers, *Polym. Eng. Sci.*, Vol 18 (No. 12), Aug 1978, p 799
5. D.W. Van Krevelen, *Properties of Polymers*, Elsevier, 1976, p 67, 395
6. *Modern Plastics Encyclopedia*, Vol 59 (No. 10A), Plastics Catalogue Corporation, Oct 1982, p 466
7. *Handbook of Chemistry and Physics*, 4th ed., Chemical Rubber Publishing Company, 1958, p 2239
8. J. Kubát and M. Rigdahl, Reduction of Internal Stresses in Injection Molded Parts by Metallic Fillers, *Polym. Eng. Sci.*, Vol 16 (No. 12), Dec 1976, p 792
9. J.V. Schmitz, Ed., *Testing of Polymers*, Vol 2, Interscience, 1966, p 208
10. J.A. Nairn and P. Zoller, Matrix Solidification and the Resulting Residual Thermal Stresses in Composites, *J. Mater. Sci.*, Vol 20, 1985, p 355
11. L.E. Nielsen, *Mechanical Properties of Polymers and Composites*, Vol 2, Marcel Dekker, 1974, p 434
12. G. Claudit, F. Disdier, and M. Locatelli, Interesting Low Temperature Thermal and Mechanical Properties of a Particular Powder-Filled Polyimide, in *Nonmetallic Materials and Composites at Low Temperatures*, A.F. Clark, R.P. Reed, and G. Hartwig, Ed., Plenum Press, 1978, p 131
13. K. Ishibashi, W. Wake, M. Kobayashi, and A. Katase, Powder-Filled Epoxy Resin Composites of Adjustable Thermal Contraction, in *Nonmetallic Materials and Composites at Low Temperatures*, Plenum Press, 1978, p 291
14. G. Hartwig and W. Weiss, Die Thermische Ausdehnung von Pulvergefüllten Epoxidharzen, *Mater. Sci. Eng.*, Vol 22, 1976, p 261
15. I.M. Daniel, Thermal Deformations and Stresses in Composite Materials, in *Thermal Stresses in Severe Environments*, Plenum Press, 1980, p 607
16. J.C.M. Li, Dislocation Dynamics in Deformation and Recovery, *Can. J. Phys.*, Vol 45, 1967, p 493
17. J. Kubát, J. Peterman, and M. Rigdahl, Internal Stresses in Polyethylene as Related to Its Structure, *Mater. Sci. Eng.*, Vol 19, 1975, p 185
18. J. Kubát and M. Rigdahl, A Simple Model for Stress Relaxation in Injection Molded Plastics With an Internal Stress Distribution, *Mater. Sci. Eng.*, Vol 21, 1975, p 63
19. L.D. Coxon and J.R. White, Residual Stresses and Aging in Injection Molded Polypropylene, *Polym. Eng. Sci.*, Vol 20 (No. 3), 1980, p 230
20. A. Bhatnagar and L.J. Broutman, Effect of Annealing and Heat Fusion on Residual Stresses in Polyethylene Pipe, in *Proceedings of the 43rd Annual Technical Conference*, Society of Plastics Engineers, 1985, p 545
21. J.G. Williams and J.M. Hodgkinson, The Determination of Residual Stresses in Plastic Pipe and Their Role in Fracture, *Polym. Eng. Sci.*, Vol 21 (No. 13), 1981, p 822
22. A. Siegmann, A. Buchman, and S. Kenig, Comments on the Layer Removal Method for Measurements of Residual Stresses in Plastics, *J. Mater. Sci. Lett.*, Vol 16, 1981, p 3514
23. A. Siegmann, S. Kenig, and A. Buchman, Residual Stresses in Polymers II: Their Effect on Mechanical Behavior, *Polym. Eng. Sci.*, Vol 21 (No. 15), 1981, p 997

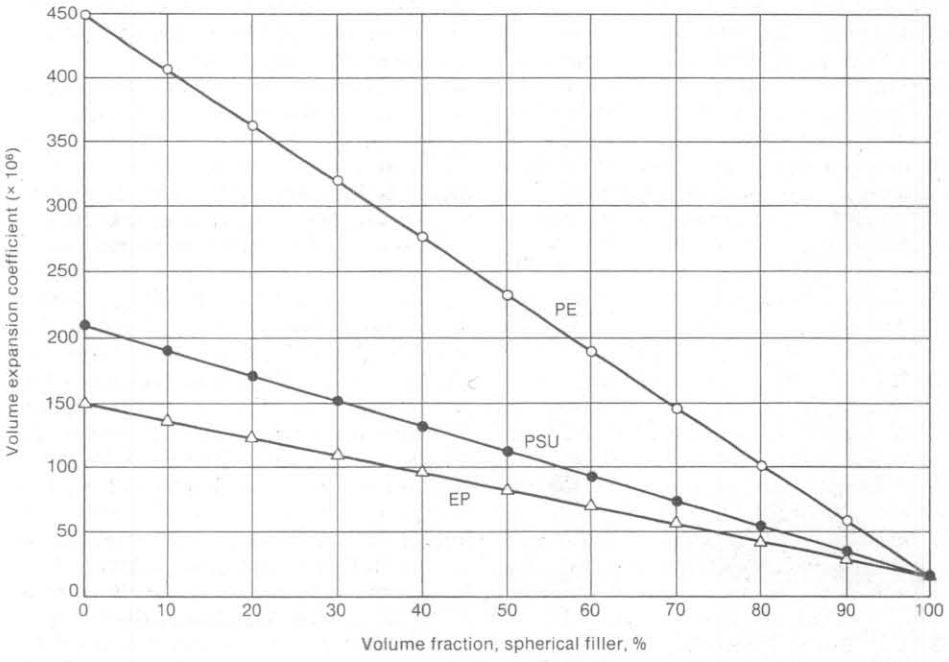

Fig. 5 Expansion coefficients, per linear rule of mixtures

24. F.R. Jones and M. Mulheron, Generation of Thermal Strains in GRP, *J. Mater. Sci. Eng.*, Vol 18, 1983, p 1533
25. M. Shimbo, M. Ochi, and K. Arai, Effect of Solvent and Solvent Concentration on the Internal Stress of Epoxide Resin Coatings, *J. Coatings Technol.*, Vol 57 (No. 728), 1985, p 93
26. J.A. Manson and J.C. Seferis, Internal Stress Determination by Process Simulated Laminates, in *Proceedings of the 45th Annual Technical Conference*, Society of Plastics Engineers, 1987, p 1446
27. I.M. Ward, Ed., *Structure and Properties of Oriented Polymers*, John Wiley & Sons, 1975
28. B.E. Read, J.C. Duncan, and D.E. Meyer, Birefringence Techniques for the Assessment of Orientation, in *Measurement Techniques for Polymer Solids*, R.P. Brown and B.E. Read, Ed., Elsevier, 1984, p 143
29. S. Raha and P.B. Bowden, Birefringence of Plastically Deformed Poly-(Methyl Methacrylate), *Polymer*, Vol 31, 1972, p 174
30. E. Saiz, E. Riande, and J.E. Mark, Birefringence in Poly(Methyl Acrylate) Networks in Elongation, *Macromolecules*, Vol 17, 1984, p 899
31. I.M. Ward, Review: The Yield Behavior of Polymers, *J. Mater. Sci.*, Vol 6, 1971, p 1397
32. A. Siegmann, S. Kenig, and A. Buchman, Residual Stresses in Injection-Molded Amorphous Polymers, *Polym. Eng. Sci.*, Vol 27 (No. 14), 1987, p 1069
33. A. Siegmann, A. Buchman, and S. Kenig, Residual Stresses in Polymers III: The Influence of Injection-Molding Process Conditions, *Polym. Eng. Sci.*, Vol 22 (No. 9), 1982, p 560
34. T. Vu-Khanh and F.X. De Charentenay, Mechanics and Mechanism of Impact Fracture in Semi-Ductile Polymers, *Polym. Eng. Sci.*, Vol 25 (No. 13), 1985, p 841
35. L. Nicolais, E. Driolo, H.B. Hopfenberg, and A. Apicella, Effects of Orientation and the Penetration Crazing and Dissolution of Polystyrene by N-Hexane, *Polymer*, Vol 20, 1979, p 459
36. A.J. Kovacs, La Contraction Isotherme du Volume des Polymères Amorphes, *J. Poly. Sci.*, Vol XXX, 1958, p 131
37. L.C.E. Struik, *Physical Aging in Amorphous Polymers and Other Materials*, Elsevier, 1978
38. S.E.B. Petrie, Thermodynamic Equilibrium in Glassy Polymers, in *Polymeric Materials*, American Society for Metals, 1973, p 55
39. Z.H. Ophir, J.A. Emerson, and G.L. Wilkes, Sub-T_g Annealing Studies of Rubber Modified and Unmodified Systems, *J. Appl. Phys.*, Vol 49 (No. 10), 1978, p 5032
40. E.S.W. Kong, S.M. Lee, and H.G. Nelson, Physical Aging in Graphite Epoxy Blends, *Polym. Compos.*, Vol 3 (No. 1), 1982, p 29
41. S. Matsuoka, Thermodynamic Aspects of Brittleness in Glassy Polymers, in *Toughness and Brittleness of Plastics*, R. Deanin and A.M. Crugnola, Ed., Advances in Chemistry Series 154, American Chemical Society, 1972, p 3
42. A.J. Kovacs, A Multiparameter Approach for Structural Recovery of Glasses and Its Implication for Their Physical Properties, in *Annals of the New York Academy of Sciences*, Vol 371, J.M. O'Reilly and M. Goldstein, Ed., New York Academy of Sciences, 1981, p 38
43. S.E.B. Petrie, Thermal Behavior of Annealed Organic Glasses, Part A-2, *J. Poly. Sci.*, Vol 10, 1972, p 1255
44. S.E.B. Petrie, The Effect of Excess Thermodynamic Properties Versus Structure Formation on the Physical Properties of Glassy Polymers, *J. Macromol. Sci. Phys.*, Vol B12 (No. 2), 1976, p 225
45. R.E. Robertson, The Aging of Glassy Polymers as Determined by Scanning Calorimeter Measurements, *J. Appl. Phys.*, Vol 49 (No. 10), 1979, p 5048
46. S.S. Sternstein, Mechanical Properties of Glassy Polymers, in *Properties of Solid Materials, Part B*, J.M. Schultz, Ed., Academic Press, 1977, p 541
47. R.A. Bubeck and S.E. Bales, Changes in Yield and Deformation of Polycarbonates Caused by Physical Aging, *Polym. Eng. Sci.*, Vol 24 (No. 10), 1984, p 1142
48. L.H. Sperling, Chapter 6, in *Introduction to Physical Polymer Science*, John Wiley & Sons, 1986, p 239
49. J.C.M. Li, Physical Chemistry of Some Microstructural Phenomena, *Metall. Trans. A*, Vol 9A (No. 10), 1978, p 1353
50. Y.P. Chen and J.J. Aklonis, Multiordering Parameter Models of Volume and Enthalpy Recovery Generalized to Treat Physical Aging: A Quantitative Investigation, *Polym. Eng. Sci.*, Vol 27 (No. 17), 1987, p 1275
51. G. Levitar and L.C.E. Struik, Physical Aging in Rigid Chain Molecules, *Polymer*, Vol 24, 1983, p 1071
52. R.P. Kambour, D. Faulkner, E.E. Kampf, S. Miller, G.E. Niznik, and A.R. Schultz, Toughness Enhancement by Introduction of Silicone Blocks Into Polycarbonates of Bisphenol Acetone and Bisphenol Fluorenone, in *Toughness and Brittleness of Plastics*, R.D. Deanin and A.M. Grugnola, Ed., Advances in Chemistry Series 154, American Chemical Society, 1976, p 312
53. R.F. Boyer, Dependence of Mechanical Properties on Molecular Motion in Polymers, *Polym. Eng. Sci.*, Vol 8 (No. 3), 1968, p 161
54. L.E. Nielsen, *Mechanical Properties of Polymers*, Vol 2, Marcel Dekker, 1974, p 165
55. J.L. Gómez and R. Díaz, Effect of the Cooling Rate in the Formation of Glass on the α and β Relaxations of Some Amorphous Polymers, *Polym. Eng. Sci.*, Vol 24 (No. 15), 1984, p 1202
56. R. Díaz and J.L. Gómez, The Influence of Thermal History of Dielectric Properties of Poly (Vinyl Chloride), *Polym. Eng. Sci.*, Vol 22, 1982, p 845
57. G.B. McKenna and A.J. Kovacs, Physical Aging of Poly (Methyl Methacrylate) in the Nonlinear Range: Torque and Normal Force Measurements, *Polym. Eng. Sci.*, Vol 24 (No. 10), 1984, p 1138
58. N. Gowri Shankar, Y.A. Bertin, and J.L. Gacougnolle, Analysis of the Evolution of Microcreep During Physical Aging and Mechanical Deformation in Poly(Methyl Methacrylate) Using A Microstructural Model, *Polym. Eng. Sci.*, Vol 24 (No. 11), 1984, p 921
59. C. Bauwens-Crowet and J.C. Bauwens, The Relationship Between the Effect of Thermal Pre-Treatment and the Viscoelastic Behavior of Polycarbonate in the Glassy State, *J. Mater. Sci.*, Vol 14, 1979, p 1817
60. T.E. Brady and G.S. Yeh, Yielding Behavior of Glassy Amorphous Polymers, *J. Appl. Phys.*, Vol 42 (No. 12), 1971, p 4622
61. J.C.M. Li and J.B.C. Wu, Pressure and Normal Stress Effects in Shear Yielding, *J. Mater. Sci.*, Vol 11, 1976, p 445
62. J.C.M. Li, Behavior and Properties of Shear Bands, *Polym. Eng. Sci.*, Vol 24 (No. 10), 1984, p 750
63. L. Camwell and D. Hull, Crazing and Fracture Associated with Interaction of Shear Bands in Polystyrene, *Philos. Mag.*, Vol 27, 1973, p 1135
64. P.B. Bowden and S. Raha, The Formation of Micro Shear Bands in Polystyrene and Polymethylmethacrylate, *Philos. Mag.*, Vol 22, 1970, p 463
65. W. Wu and A.P.L. Turner, Shear Bands in Polycarbonate, *J. Polym. Sci.*, Vol 11, 1973, p 2199
66. S.P. Chen, Effect of Volume Relaxation, Temperature and Chemical Structure on Diffusion of Gaseous Hydrocarbons Through Glassy Polymers, *Polym. Preprints*, Vol 51 (No. 1), 1974, p 71
67. H.B. Hopfenberg, V.T. Stannett, and G.M. Folk, Sorption Kinetics and Equilibria in Annealed Glassy Polyblends, *Polym. Eng. Sci.*, Vol 15 (No. 4), 1975, p 261